

Identification of mechanistic CKD biomarkers in a rat SNx kidney fibrosis model by transcriptomics and proteomics detectable in biofluids

Karin Barnouin, Elisa Tonoli, Clare Coveney, John Atkinson, Margarida Sancho, Andrew Skelton, David J Boockock, Linghong Huang, Joseph Shephard, Tim Johnson, Elisabetta AM Verderio, and Breda Twomey

Supplementary Methods

Subtotal Nephrectomy rat model generation

Animals were housed in open-top cages, in a specific-pathogen-free facility according to the Federation of European Laboratory Animal Science Associations recommendations. Typically, animals were housed in groups of four or five. Food (RM1; SAFE, Paris, France) and water (untreated mains tap water) were available ad libitum, and the light cycle was 12/12 hours light and dark. Room temperature and humidity were 21°C and 45%, respectively. Nest building material was provided, and all cages contained enrichment such as a red translucent house, a wheel and a tunnel.

Prior to surgery, male Wistar rats (200-300g) were acclimatised to the facility for one week. They were then dosed with pre-operative analgesia (0.01mg/kg Buprenorphine) and anaesthetised with isoflurane. The left flank was then shaved, the animals dosed with pre-operative carprofen (5mg/kg) and the animals transferred to the surgery suite. The animals were placed on an isoflurane nose-cone, covered with a sterile drape, and eye ointment was applied to prevent drying. The surgical site was cleaned and disinfected, and an incision made through the skin, and then blunt dissection was used to part the muscle later. The left kidney was decapsulated and the renal blood vessels clamped. The poles of the kidney were ligated using 3-0 mersilk sutures, and then excised using a scalpel. 3M tissue glue was applied to the cut ends. The clamp was then removed, and the kidney replaced into the abdomen. The muscle was sutured using 5-0 Vicryl in a continuous pattern, and the skin was sutured using 5-0 Vicryl in a sub-cuticular continuous pattern. Local anaesthetic (marcain (0.5mg/kg) was applied to the surgical site. Animals were allowed to recover on a warming rack and monitored for welfare. Animals received post-operative analgesia for 4 days.

One week later, the animals were prepared for surgery as above, and the right kidney decapsulated and clamped. The right renal blood vessels were ligated using 3-0 mersilk, and the entire right kidney removed. Animals were sutured as above, and allowed to recover as above, with post-operative analgesia for 4 days.

Animals were tail-pricked or bled (30 µL) for twice-weekly serum creatinine measurements and were placed in metabolic cages bi-weekly for proteinuria measurements. The animals were allocated to a study group in a random manner using a random number generator once they reached the threshold of 2-fold increase in serum creatinine and 3-5x fold increase in proteinuria compared to non-operated sham control. Animals were anaesthetised, bled by cardiac puncture, terminated by cervical dislocation, death confirmed, and the kidney remnant removed, cut into quarters, and either fixed in formalin or snap frozen in liquid nitrogen.

Analysis was performed in a blinded manner, with the analyst and the interpreting researcher unaware of which animals were sham or subtotal nephrectomy-operated.

UUO mouse model generation

UUO surgery was performed on male C57Bl6/J mice of between 20-30g body weight.

Prior to surgery, all animals are dosed with 100 µL pre-operative Buprenorphine (0.05mg/kg Mice / 0.01mg/kg Rats). Mice are anaesthetised with isoflurane and a small patch of skin shaved just below the ribs on the left flank. Mice are then dosed with pre-operative carprofen (5mg/kg). The mouse is laid on the operating table on a sterile drape under isoflurane anaesthesia. The surgical site is disinfected with chlorhexidine and the animal covered by a sterile drape. A small incision is made below the ribcage, parallel to the spine, the muscle is exposed by blunt dissection and a small incision made. The opening in the muscle is widened using blunt dissection. The ureter is located and ligated using 2x 3-0 Mersilk (Ethicon). The ureter is replaced, and the muscle sutured using 5-0 Vicryl (Ethicon). The skin is then sutured in a sub-cuticular pattern with 5-0 Vicryl (Ethicon). The wound is cleaned with chlorhexidine and levobupivacaine administered to the site (0.5mg/kg). Surgical duration is approximately 15-20 minutes, and animals are monitored throughout for surgical anaesthetic plane. Animals were returned to their home cage and received post-operative analgesia for 4 days (Buprenorphine and Carprofen at the doses above). All mice were housed under specific pathogen-free conditions and maintained on a 12- hour light/dark cycle with free access to food and water.

Animals were monitored daily for welfare scoring and body weight. At Day 21 animals were terminated by a schedule 1 method and tissues harvested.

Adriamycin mice model generation:

The Adriamycin model was performed on male BalbC mice of between 20-30g body weight.

A dose of 10.5mg/kg Adriamycin was administered via the tail vein of unanaesthetised mice. Animals were returned to their home cage and monitored daily for welfare scoring and body weight. Urine was collected prior to termination using a metabolic cage. Termination was performed by a schedule 1 method at day 14 and tissues collected. All mice were housed under specific pathogen-free conditions and maintained on a 12- hour light/dark cycle with free access to food and water. 24-hour urine samples were collected prior to injection of Adriamycin and termination, so there were 2 urine collections per animal.

Collagen Picrosirius Red (PSR) Staining

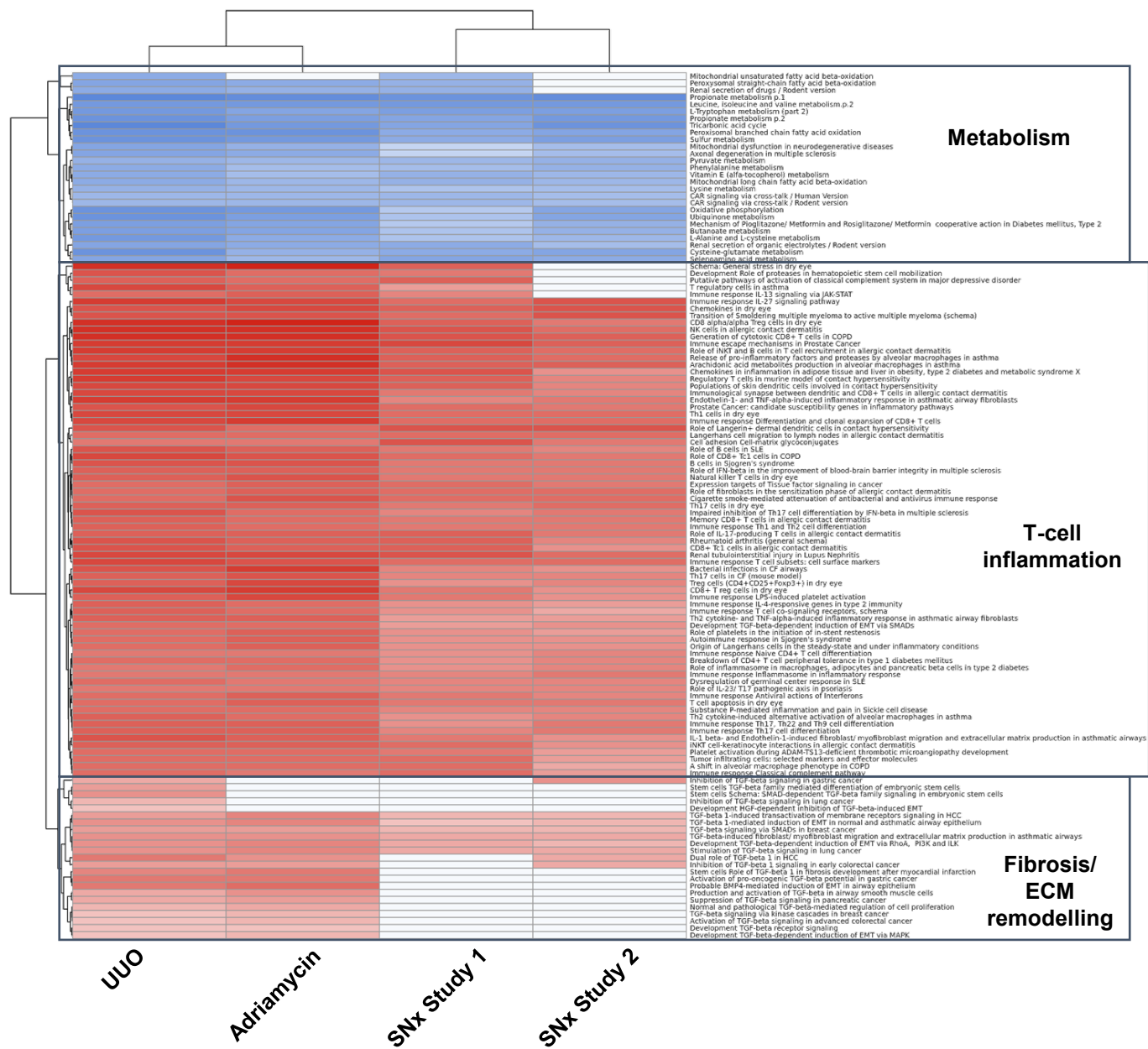
Kidney samples were harvested and fixed in 10% formalin for 24 hours. The samples were coded for blinding and placed in a labelled cassette, which entails further formalin fixation, dehydration in increasing concentrations of alcohol, clearing in xylene and impregnation with paraffin wax. After this, samples were orientated in paraffin wax with the cassette placed on top of the embedding moulds. The kidney samples were sectioned at 3 µm using a Leica Histocore multicut. These sections were floated onto a warm water bath and were placed onto labelled Superfrost Plus Gold slides for staining. The slides were de-waxed and hydrated.

Nuclei were stained with Weigert's haematoxylin for 8 minutes, and then the slides washed for 10 minutes in running tap water. The slides were stained in picro-sirius red solution for one hour, and then washed in two changes of acidified water. Water was removed, and the slides dehydrated in 100% alcohol. The slides were then cleared with xylene, and coverslips applied. Whole slides were then scanned using an OlyVIA slide scanner (Olympus) and given codes for the blinding of the image analysis.

Image Analysis

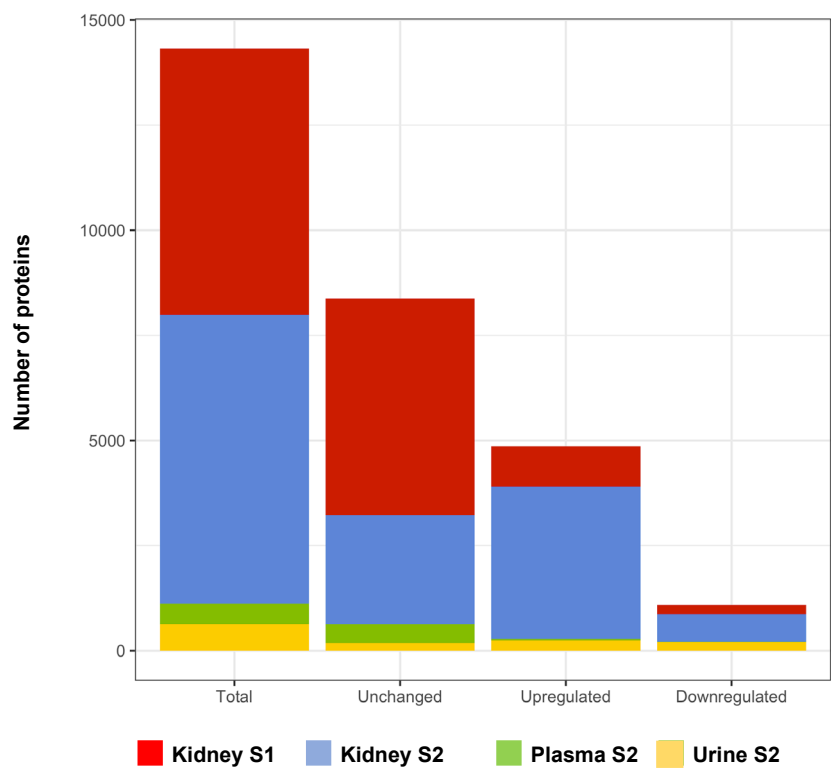
Whole slide scans were uploaded to VisioPharm Image analysis software. In a blinded manner, the cortices of the kidneys were manually annotated, excluding the medulla from analysis. Thresholds were set for detecting red-stained collagen and the software allowed to run this detection over the entire cortex of each kidney. Data were outputted as the percentage area of the renal cortex that stained positive for collagen / PSR staining.

Supplementary Figure 1



Supplementary figure 1: Comparison of transcriptomics profiles of rat SNx with other CKD models.

Supplementary Figure 2

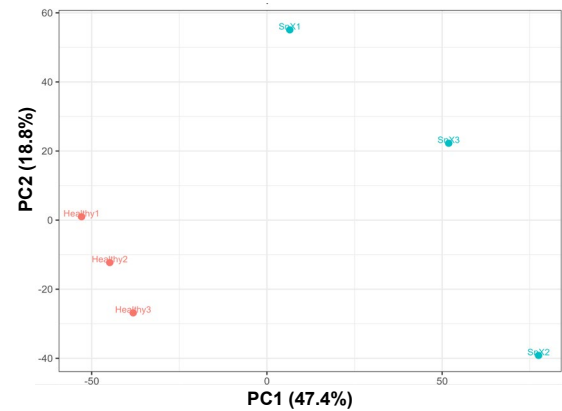


Supplementary figure 2: Summary of protein counts

Supplementary Figure 3

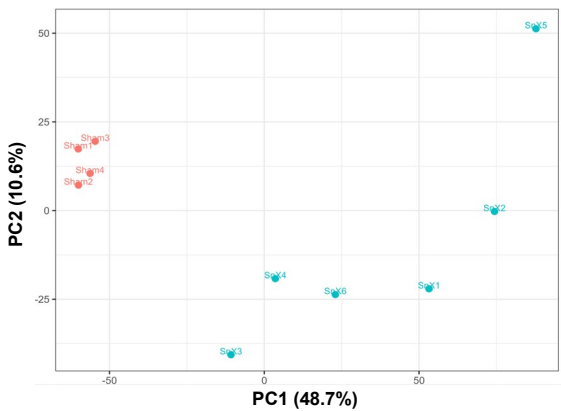
Kidney – Study 1

● Sham ● SNx



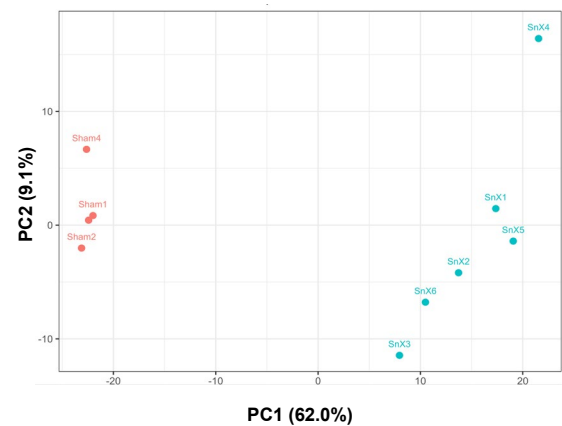
Kidney – Study 2

● Sham ● SNx



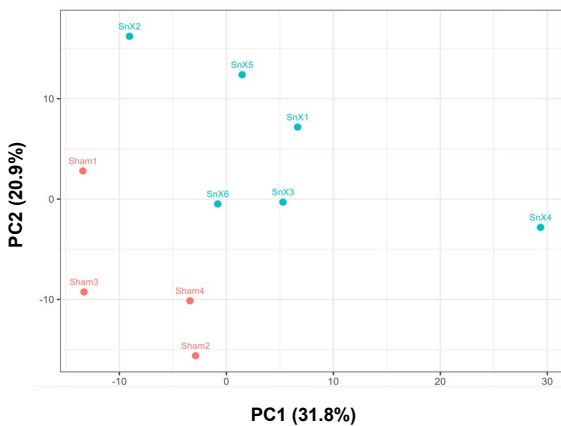
Urine – Study 2

● Sham ● SNx



Plasma – Study 2

● Sham ● SNx



Supplementary Figure 3: PCA analysis of proteomic data.

Supplementary Figure 4

Supplementary figure 4: TreeMaps Biological Processes GO enriched in unsupervised cluster analysis – DAVID – KEGG of proteomic data

a

[illegible][illegible]

b

fatty acid metabolic process, 66	gluconeogenesis, 62	NAD(P) metabolic process, 60	glutathione biosynthetic process, 58	response to oxidative stress, 65	response to aluminum ion, 53	response to activity, 50	liver development, 56	regulation of acetyl-CoA biosynthetic process from pyruvate, 36	regulation of vacuole fusion, non-autophagic, 36
ubiquinone biosynthetic process, 57	isocitrate metabolic process, 47	transsulfuration, 47	proton motive force-driven mitochondrial ATP synthesis, 43	response to oxidative stress			liver development	regulation of vacuole fusion, non-autophagic	regulation of vacuole fusion, non-autophagic
one-carbon metabolic process, 55	urate metabolic process, 40	methyl-branched fatty acid metabolic process, 40	nitric oxide biosynthetic process, 38	4-hydroxyproline catabolic process, 36	cellular oxidant detoxification, 63	response to starvation, 34	response to isolation stress, 18	cellular response to hypoxia stimulus, 8	regulation of microvillus length, 21
					response to ethanol, 22	cellular response to hypoxia stimulus, 8	positive regulation of nuclear-cytosol transport, 8	regulation of macroautophagy, 19	
hydrogen peroxide catabolic process, 52	nucleobase-containing compound metabolic process, 35	phosphorylation, 30	ketone body biosynthetic process, 24	succinyl-CoA catabolic process, 24	protein homotetramerization, 61	brush border assembly, 36	mitochondrial respiratory chain complex I assembly, 25	nitrogen compound metabolic	lipid metabolic process
	bile acid biosynthetic process, 33	branched-chain amino acid catabolic process, 28	amine metabolic process, 18	proteolysis, 17	mitochondrion organization, 42	actin filament bundle assembly, 20	peroxisome fission, 13	nitrogen compound metabolic process	cell redox homeostasis
succinyl-CoA metabolic process, 49	3'-phosphoadenosine 5'-phosphosulfate metabolic process, 31	2-oxoglutarate metabolic process, 27	heme biosynthetic process, 15	amide catabolic process, 8	carbon dioxide transport, 46	nitric oxide transport, 32	glucose transmembrane transport, 15	carbohydrate metabolic process	carbamate metabolic process, CoA-linked
	ethanol catabolic process, 10	ethanol catabolic process, 10	heme biosynthetic process, 15	amide catabolic process, 8	proton transmembrane transport			generation of precursor metabolites and energy	glutathione metabolic process
					amino acid transport, 44	proton transmembrane transport, 29	modified amino acid transport, 8	generation of precursor metabolites and energy, 48	cellular aldehyde metabolic process
							protein localization to microvillus, 8		glutathione metabolic process
							transcriptional activator transport, 3		adaptive thermogenesis

regulation of catalytic activity, 148	complement activation, 145	positive regulation of cell migration, 144	regulation of alternative mRNA splicing, via spliceosome, 141	positive regulation of substrate adhesion-dependent cell spreading, 140	macroautophagy, 149	mRNA splicing, via spliceosome, 127	proteolysis, 126	protein phosphorylation, 124	peptidyl-threonine phosphorylation, 116	vesicle-mediated transport, 134	vesicle docking involved in exocytosis, 119	endothelial cell differentiation, 143	aging, 142
negative regulation of apoptotic process, 137	positive regulation of telomerase RNA localization to Cajal body, 136	response to endoplasmic reticulum stress, 133	response to xenobiotic stimulus, 132	regulation of nucleotide-excision repair, 131	7-methylguanine cap hypermethylation, 115	transcription elongation by RNA polymerase II, 101	peptidyl-serine phosphorylation, 100	fructose 6-phosphate metabolic process, 96	protein processing, 94	receptor-mediated endocytosis, 112	toxin transport, 103	osteoblast differentiation, endodermal cell differentiation, 90	liver regeneration, 140
response to hypoxia, 130	positive regulation of protein localization to Cajal body, 124	response to calcium ion, 123	regulation of G0 to G1 transition, 121	cellular response to interleukin-7, 120	phosphatidylinositol biosynthetic process, 108	mRNA splicing, via spliceosome glycosylation, 85	GMP biosynthetic process, 58	RNA secondary structure unwinding, 58	membrane protein ectodomain proteolysis, 63	protein transport, 89	protein localization to bicellular tight junction, 80	maintenance of blood-brain barrier, 84	tissue remodeling, 58
regulation of cell shape, 118	negative regulation of nitric oxide biosynthetic process, 97	regulation of macroautophagy, protein stabilization, 97	regulation of cell cycle arrest, 92	positive regulation of miRNA-mediated gene silencing, 91	regulation of transcription elongation by RNA polymerase II, 90	receptor catabolic process, 83	peptidyl-lysine hydroxylation, 72	DNA metabolic process, 68	histone H2B ubiquitination, 23	protein localization to bicellular tight junction, 80	protein localization to bicellular tight junction, 80	ossification, 66	osteoblast differentiation, 66
positive regulation of receptor-mediated endocytosis, 117	acute-phase response, 87	intracellular signal transduction, 75	regulation of RNA splicing, 73	stress-activated MAPK cascade, 71	positive regulation of viral genome replication, 69	cytoplasmic translation, 107	protein autophagy, 82	translational initiation, 53	histone H2B ubiquitination, 23	cell-cell adhesion, 130	viral entry into host cell	cell division division, 130	localization localization, 122
regulation of circadian rhythm, 109	regulation of cell population proliferation, 86	post-transcriptional regulation of gene expression, 62	response to ischemia, 56	regulation of translational initiation, 42	positive regulation of G0G1 transition, 37	Golgi organization, 146	lamellipodium assembly, 128	nucleus organization, 102	extracellular matrix disassembly, 88	apoptotic process	cell cycle	rhythmic process	cell motility motility, 105
negative regulation of protein ubiquitination, 104	positive regulation of superoxide anion generation, 79	regulation of protein complex stability, 61	cellular response to nitrogen starvation, 55	cellular senescence, 37	positive regulation of receptor signaling, 32	chromatin remodeling, 138	actin filament organization assembly, 121	membrane fusion with vacuole, 74	clathrin coat assembly, 64	chaperone-mediated protein folding	fructose 1,6-bisphosphate metabolic process	establishment or maintenance of cell polarity	protein folding
Rac protein signal transduction, 102	negative regulation of intracellular receptor signaling pathway, 78	regulation of protein complex stability, 61	cellular response to nitrogen starvation, 55	cellular senescence, 37	positive regulation of receptor signaling, 32	membrane fission, 135	supramolecular fiber organization, 106	telomere maintenance via telomerase, 70	ESRRT II complex formation, 44	mitochondrial cell mitotic cell cycle, 111	cell population proliferation	collagen biosynthetic process	metabolic process

Supplementary figure 4b: TreeMaps of down- and up-regulated proteins enriched in Kidney Study 2

C

retina homeostasis, 27		T cell activation, 20		glycosaminoglycan catabolic process, 26		proteolysis, 17		cell adhesion		actomyosin structure organization, 13	
retina homeostasis				glycosaminoglycan catabolic process						actomyosin structure organization	
detection of chemical stimulus involved in sensory perception of bitter taste, 22		metanephric distal convoluted tubule development, 12		peptide catabolic process, 19		oligosaccharide catabolic process, 8		protein processing, 3		regulation of microvillus length, 11	
		amyloid-beta clearance, 5									
		locomotory apparatus balance, 1									
folate import across plasma membrane, 23		receptor-mediated endocytosis, 16		positive regulation of antibacterial peptide production, 12		positive regulation of protein localization to early endosome, 10		carbohydrate metabolic process, 24		viral entry into host cell	
folate import across plasma membrane				positive regulation of antibacterial peptide production		cellular response to steroid hormone stimulus, 19		carbohydrate metabolic process			
lysosomal transport, 18		protein localization to plasma membrane, 14		negative regulation of endopeptidase activity, 9		cellular response to complement-dependent cytotoxicity		leukocyte cell-cell adhesion		cell migration	
		intracellular cholesterol transport, 5		regulation of cell shape, 6		response to wounding, 7				cholesterol metabolic processes	
				negative regulation of							

positive regulation of CoA-transferase activity, 45	acute-phase response, 44	positive regulation of substrate adhesion-dependent cell spreading, 42	positive regulation of receptor-mediated endocytosis, 41	reverse cholesterol transport, 46	iron ion transport, 31	plasminogen activation, 47	proteolysis, 43
				reverse cholesterol transport		plasminogen activation	
				phospholipid efflux, 38	vitamin transport, 30	lipoprotein metabolic process, 28	protein oxidation, 9
					transport, 11		
response to xenobiotic stimulus, 39	negative regulation of endopeptidase activity, 29	regulation of glucose metabolic process, 27	negative regulation of macrophage derived foam cell differentiation, 26	phosphatidylinositol 3-kinase signaling, 24			
	negative regulation of endopeptidase activity						
	blood coagulation, 22	ERK1 and ERK2 cascade, 19	cellular response to amino acid stimulus, 16	regulation of peptidyl-tyrosine phosphorylation, 15	collagen fibril organization, 37	cell adhesion	hyaluronan metabolic process
negative regulation of very-low-density lipoprotein particle remodeling, 34					collagen fibril organization		
	complement activation, 21	positive regulation of superoxide anion generation, 18	integrin-mediated signaling pathway, 14	response to mechanical stimulus, 13	protein polymerization, 35		
				negative regulation of estradiol-dependent signaling pathway via death domain receptors, 12	high-density lipoprotein particle remodeling, 35	triglyceride homeostasis	cholesterol metabolic process
liver regeneration, 32	positive regulation of cell migration, 20	in utero embryonic development, 17	response to nutrient, 10	ossification, 7			
			regulation of extracellular matrix assembly, 9	positive regulation of lipid catabolic process, 8	cytolysis	cell-matrix adhesion	type B pancreatic cell proliferation
				negative regulation of cell population proliferation, 6			

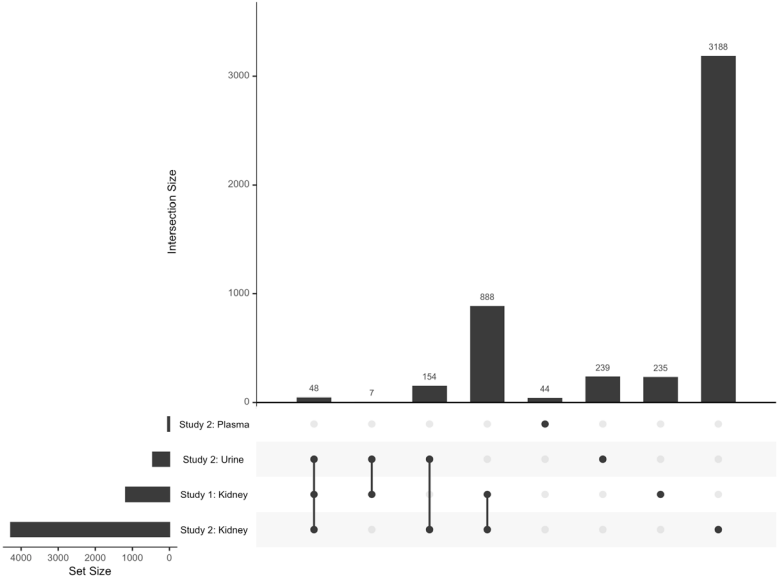
complement activation, 34	regulation of apoptotic process, 24	negative regulation of endothelial cell migration, 23	positive regulation of neurofibrillary tangle assembly, 22			lipoprotein metabolic process, 32		protein oxidation, 19	reverse cholesterol transport, 33	
high-density lipoprotein particle clearance, 31	positive regulation of low-density lipoprotein particle receptor catabolic process, 21	positive regulation of amyloid fibril formation, 18	positive regulation of cholesterol metabolic process, 18	blood coagulation, fibrin clot formation, 16		lipoprotein metabolic process			reverse cholesterol transport	
	complement activation					lipoprotein biosynthetic process, 18		peptidyl-methionine modification, 17	phospholipid efflux, 26	
positive regulation of CoA-transferase activity, 30	response to glucocorticoid, 20	female pregnancy, 15	nitric oxide mediated signal transduction, 11	positive regulation of amyloid-beta formation, 10					protein import, 18	
		regulation of Cdc42 protein signal transduction, 14	inflammatory response, 9	intrinsic apoptotic signaling pathway, 6	protein stabilization, 5	triglyceride metabolic process, 27			cholesterol homeostasis	actin filament organization
negative regulation of endopeptidase activity, 29	positive regulation of phospholipid efflux, 19	kidney development, 13	aging, 7	negative regulation of endothelial cell proliferation, 4	positive regulation of nitric oxide biosynthetic process, 2	triglyceride metabolic process				
				vasodilation, 3	response to xenobiotics stimulus, 3	cholesterol metabolic process, 25				
									cytolysis	

Supplementary figure 4c: TreeMaps of down- and up-regulated proteins in Study 2 Plasma and Urine

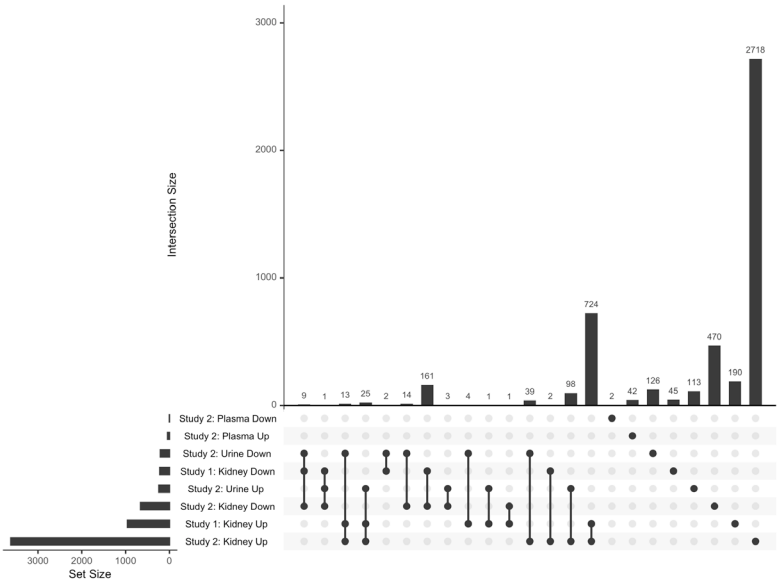
Supplementary

Figure 5

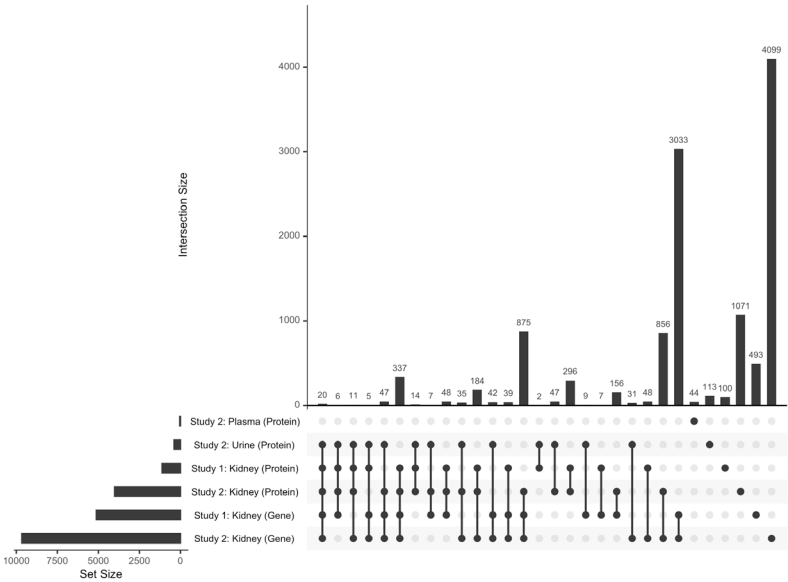
a



b



c



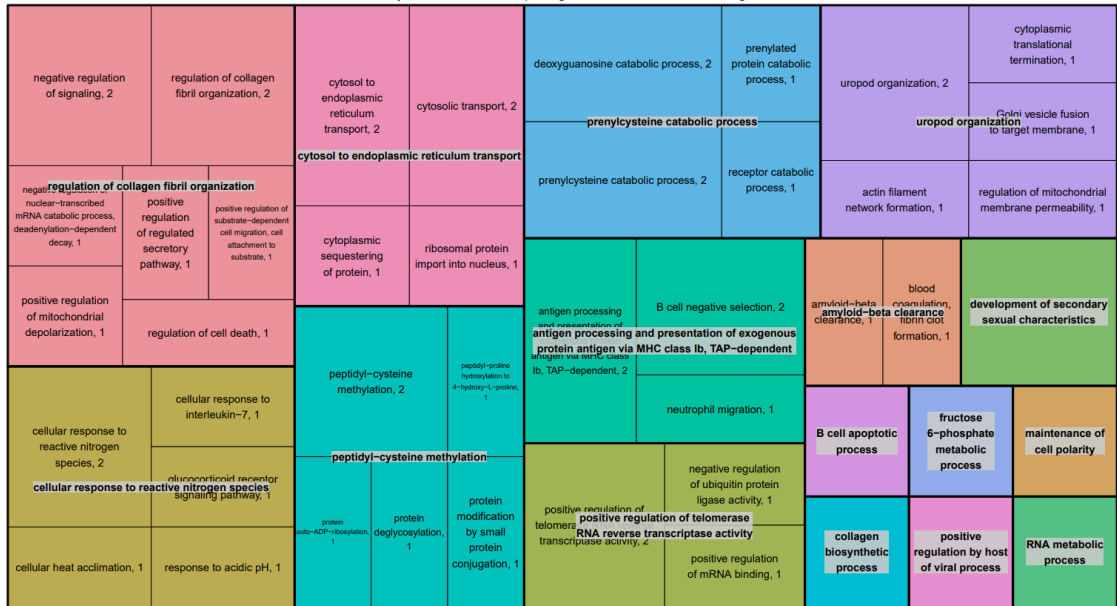
Supplementary figure 5: Upset plots comparing different tissues or analyses. a) Proteomics intersections in Kidneys, Plasma and Urine (total numbers). **b)** Proteomics intersections in Kidneys, Plasma and Urine (significantly changed proteins). **c)** Proteomics and transcriptomics intersections in Kidneys, Plasma and Urine (total numbers).

Supplementary Figure 6

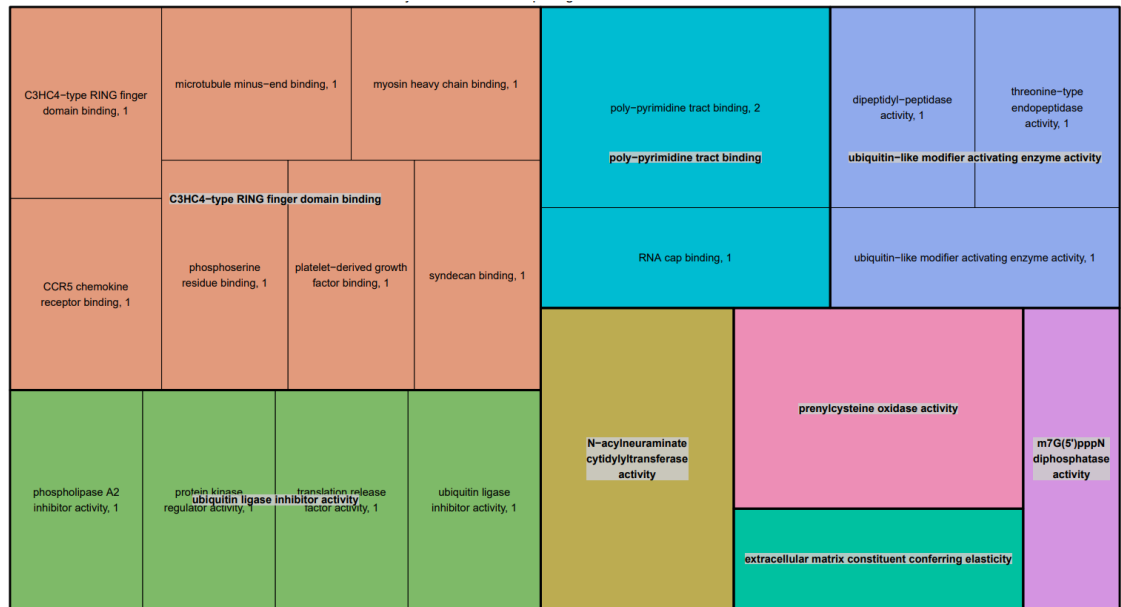
Supplementary Figure 6: TreeMaps GO (Biological processes, Molecular Function and Cellular Component) enriched in unsupervised cluster analysis – DAVID in proteomic and transcriptomic datasets. a) GO enriched in up-regulated proteins in both Kidney Studies 1 and 2. **b)** GO enriched in down-regulated proteins in both kidney Studies 1 and 2. **c)** GO enriched in up-regulated proteins in both Study 2 kidney and urine. **d)** GO enriched in down-regulated proteins in both Study 2 kidney and urine. **e)** GO enriched in down-regulated proteins and genes in both Study 1 kidney proteomic and transcriptomics datasets. **f)** GO enriched in down-regulated proteins and genes in both Study 2 kidney proteomic and transcriptomics datasets. **g)** GO enriched in down-regulated proteins and genes in both Studies 1 and 2 kidney proteomic and transcriptomics datasets.

a

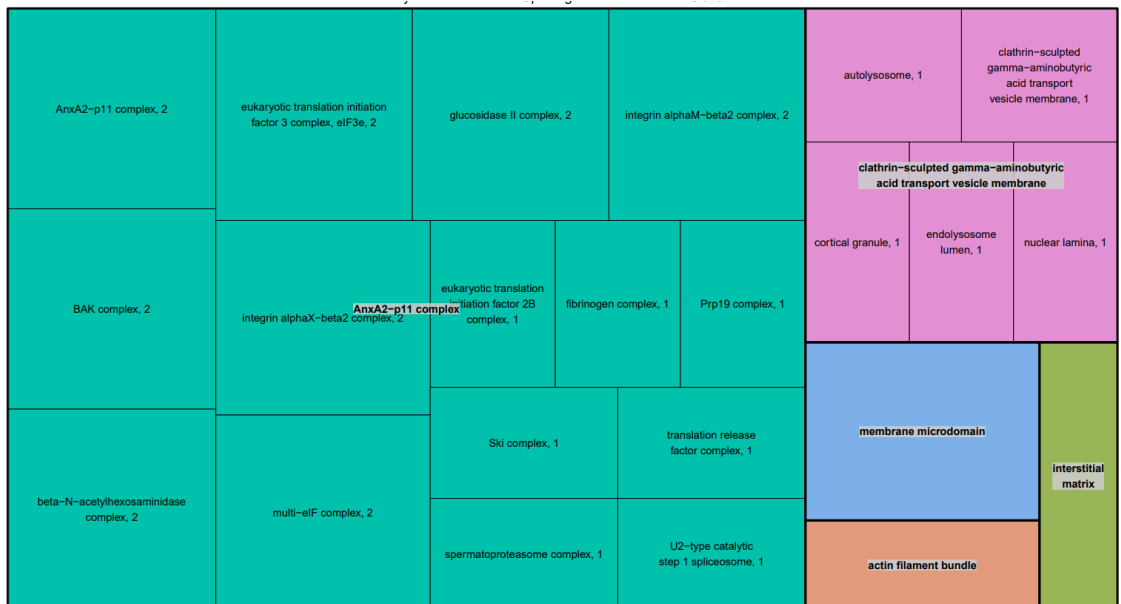
Proteomics Kidneys Studies 1 & 2 Up-Regulated Intersection GO Biological Processes



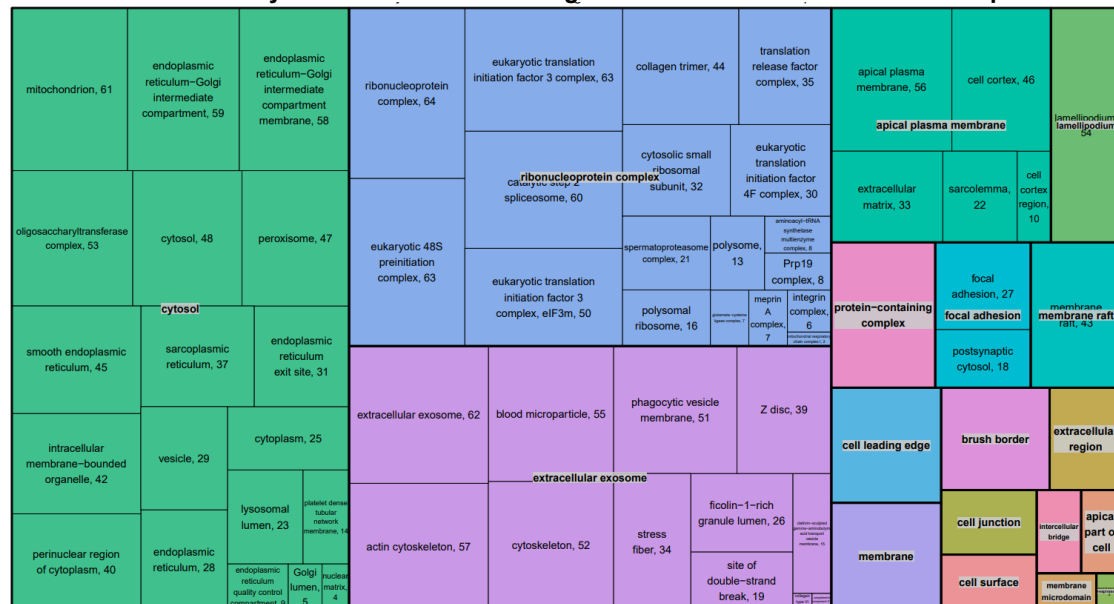
Proteomics Kidneys Studies 1 & 2 Up-Regulated Intersection GO Molecular Function



Proteomics Kidneys Studies 1 & 2 Up-Regulated Intersection GO Cellular Component

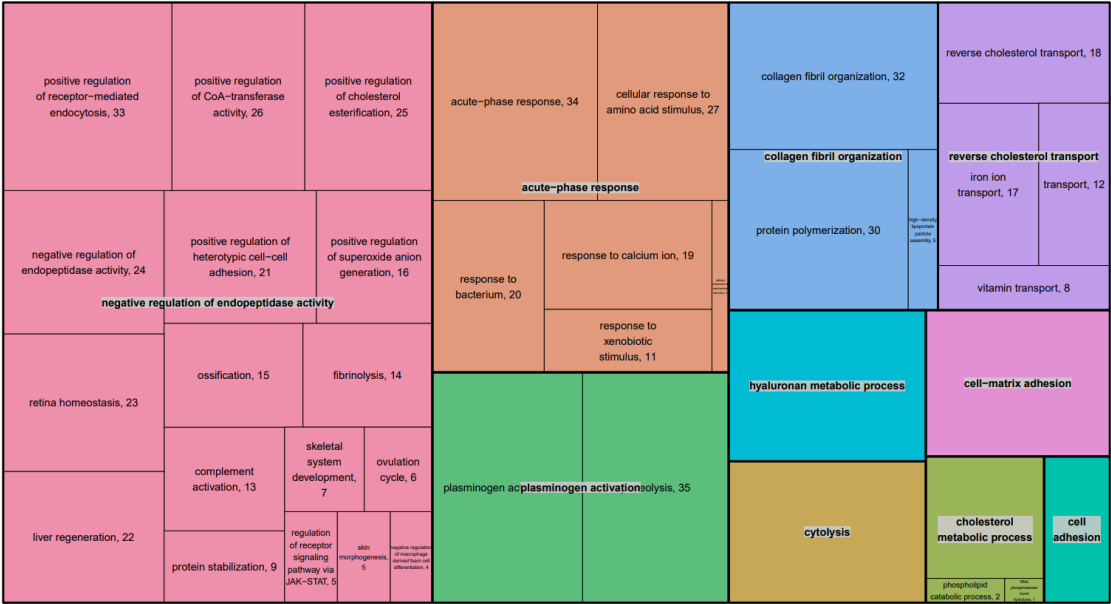


Proteomics Kidneys Studies 1 & 2 Down-Regulated Intersection GO Biological Processes

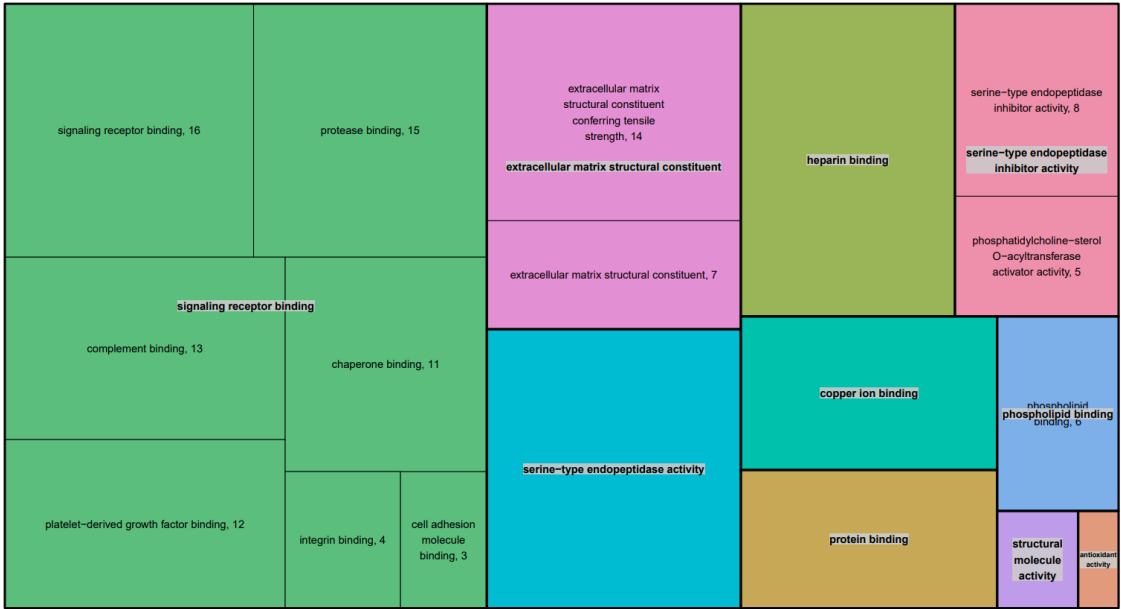


C

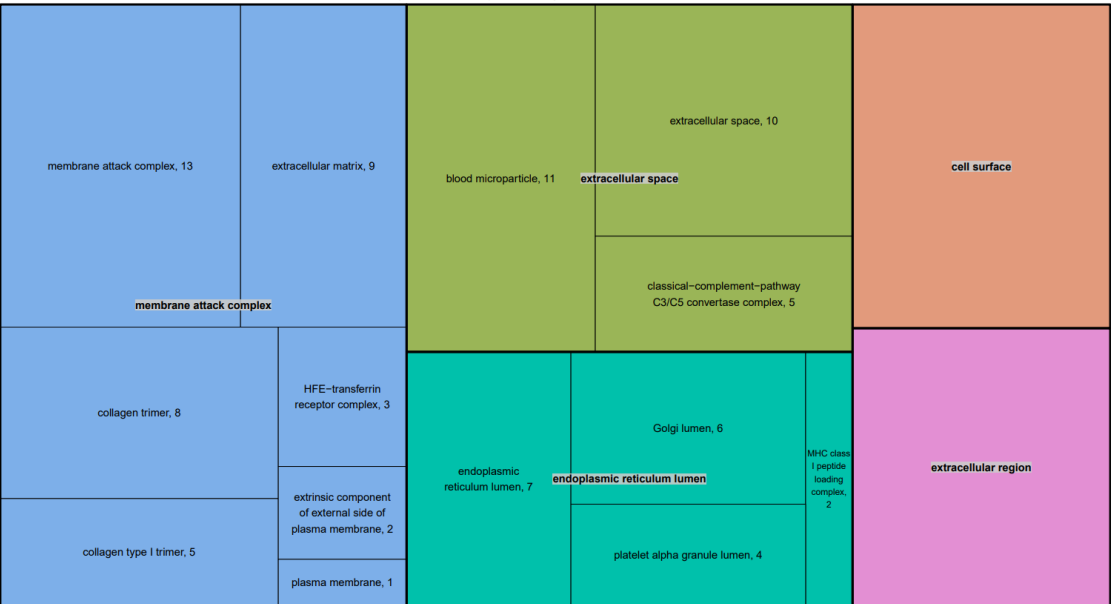
Proteomics Kidney & Urine Study 2 Up-Regulated Intersection GO Biological Processes



Proteomics Kidney & Urine Study 2 Up-Regulated Intersection GO Molecular Function



Proteomics Kidney & Urine Study 2 Up-Regulated Intersection GO Cellular Component



d

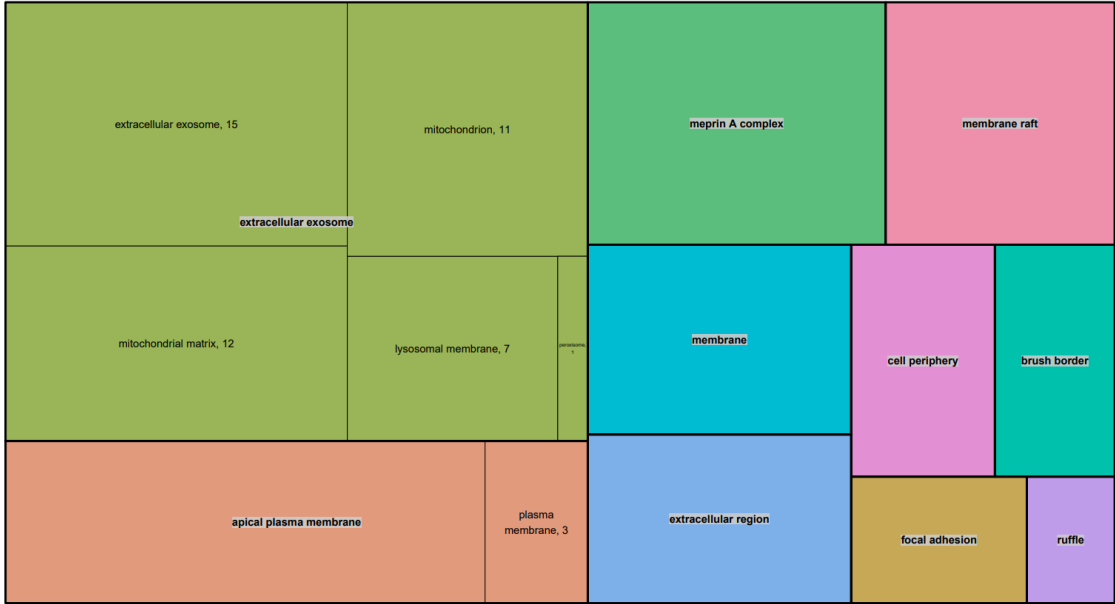
Proteomics Kidney & Urine Study 2 Down-Regulated Intersection GO Biological Processes



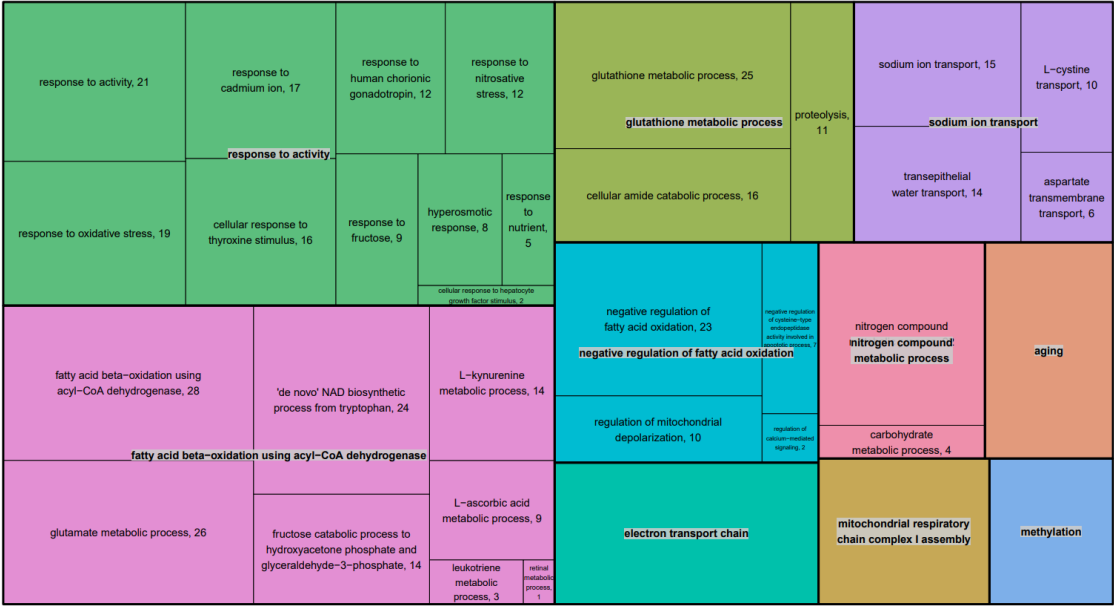
Proteomics Kidney & Urine Study 2 Down-Regulated Intersection GO Molecular Function



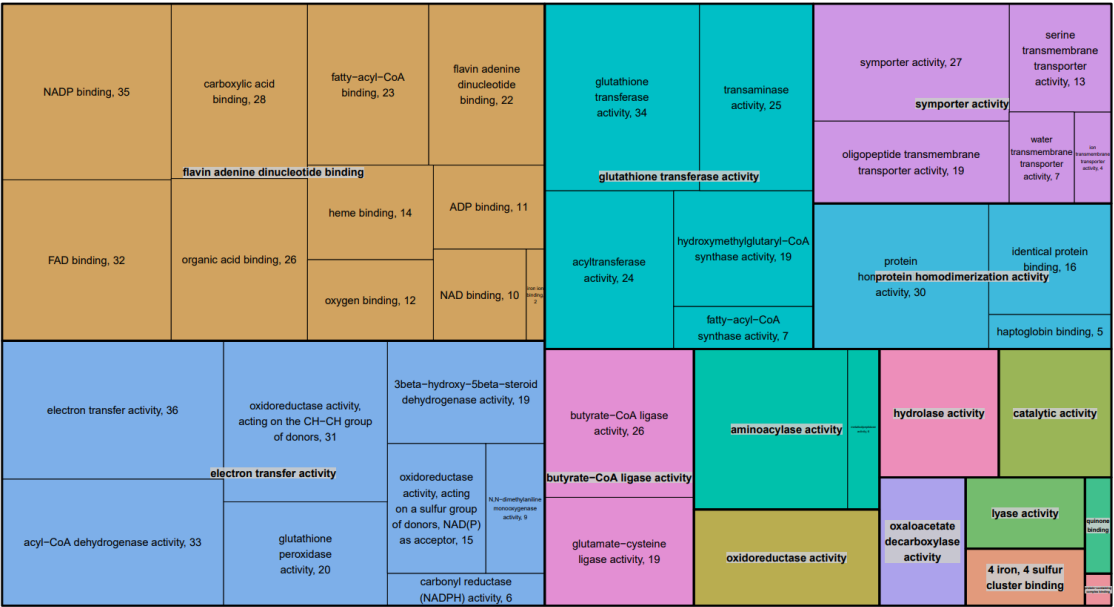
Proteomics Kidney & Urine Study 2 Down-Regulated Intersection GO Cellular Component



e Kidney Study 1 Proteomics and Transcriptomics Down-Regulated Intersection GO Biological Processes



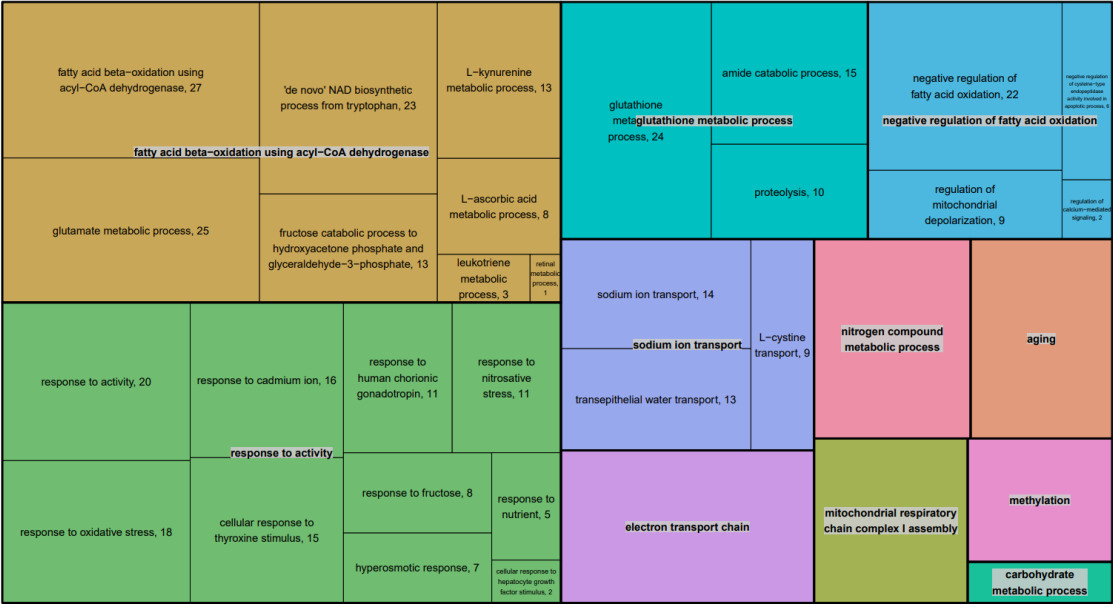
Kidney Study 1 Proteomics and Transcriptomics Down-Regulated Intersection GO Molecular Function



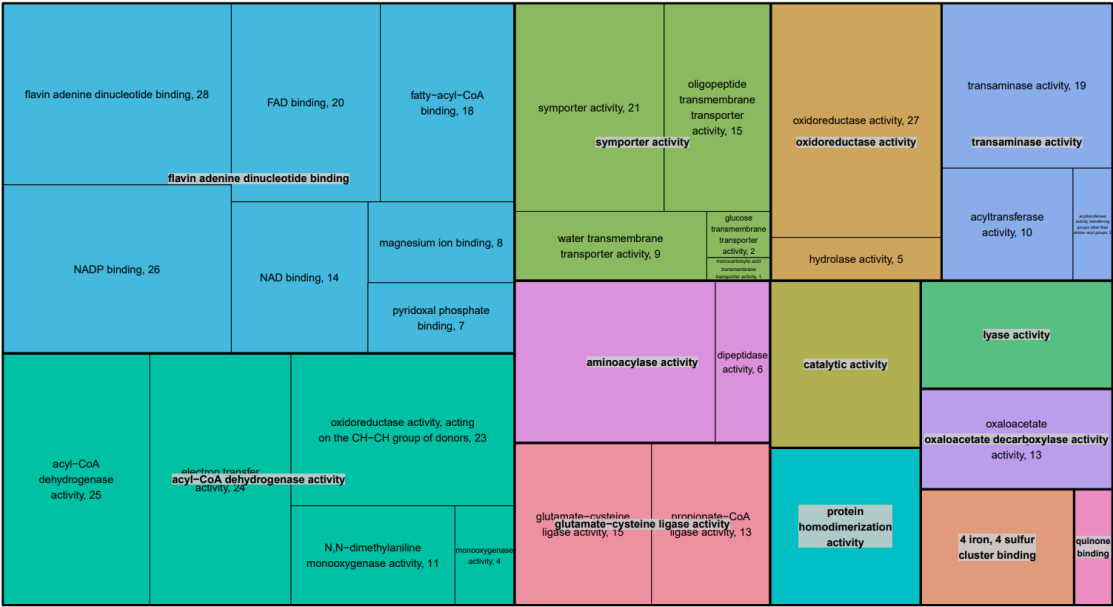
Kidney Study 1 Proteomics and Transcriptomics Down-Regulated Intersection GO Cellular Component



g Proteomics and Transcriptomics Kidney Studies 1&2 Down-Regulated Intersection GO Biological Processes



Proteomics and Transcriptomics Kidney Studies 1&2 Down-Regulated Intersection GO Molecular Function

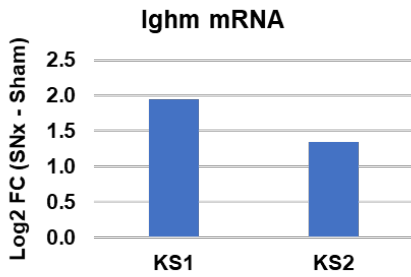
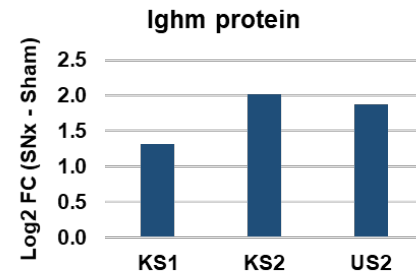
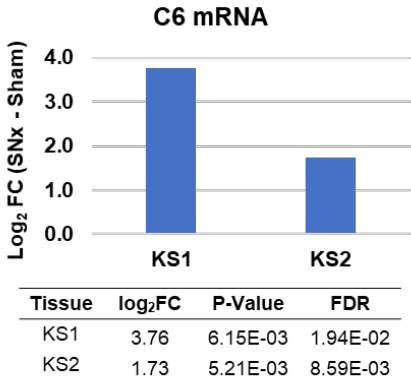
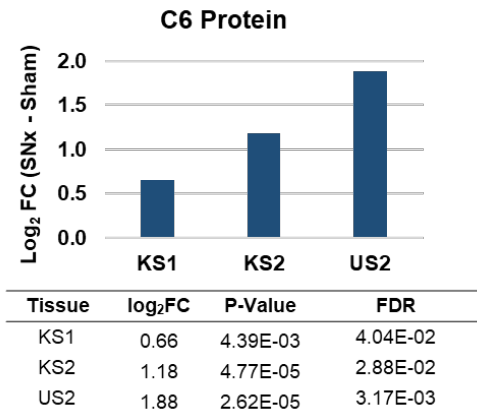
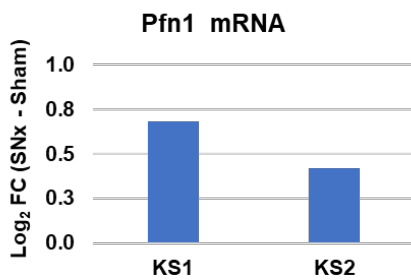
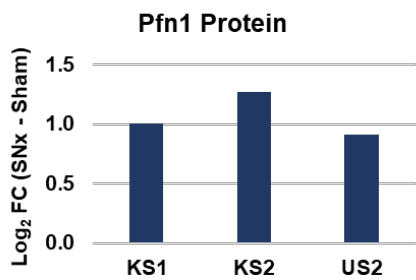
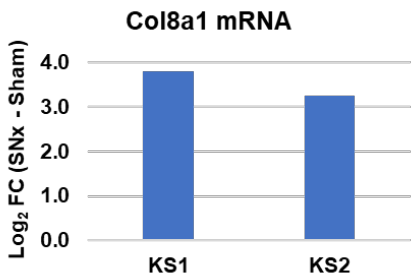
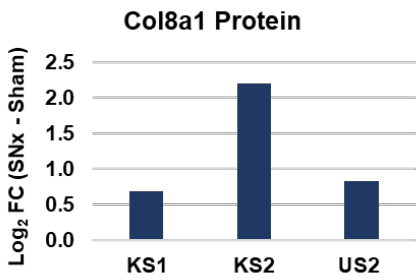


Proteomics and Transcriptomics Kidney Studies 1&2 Down-Regulated Intersection GO Cellular Component

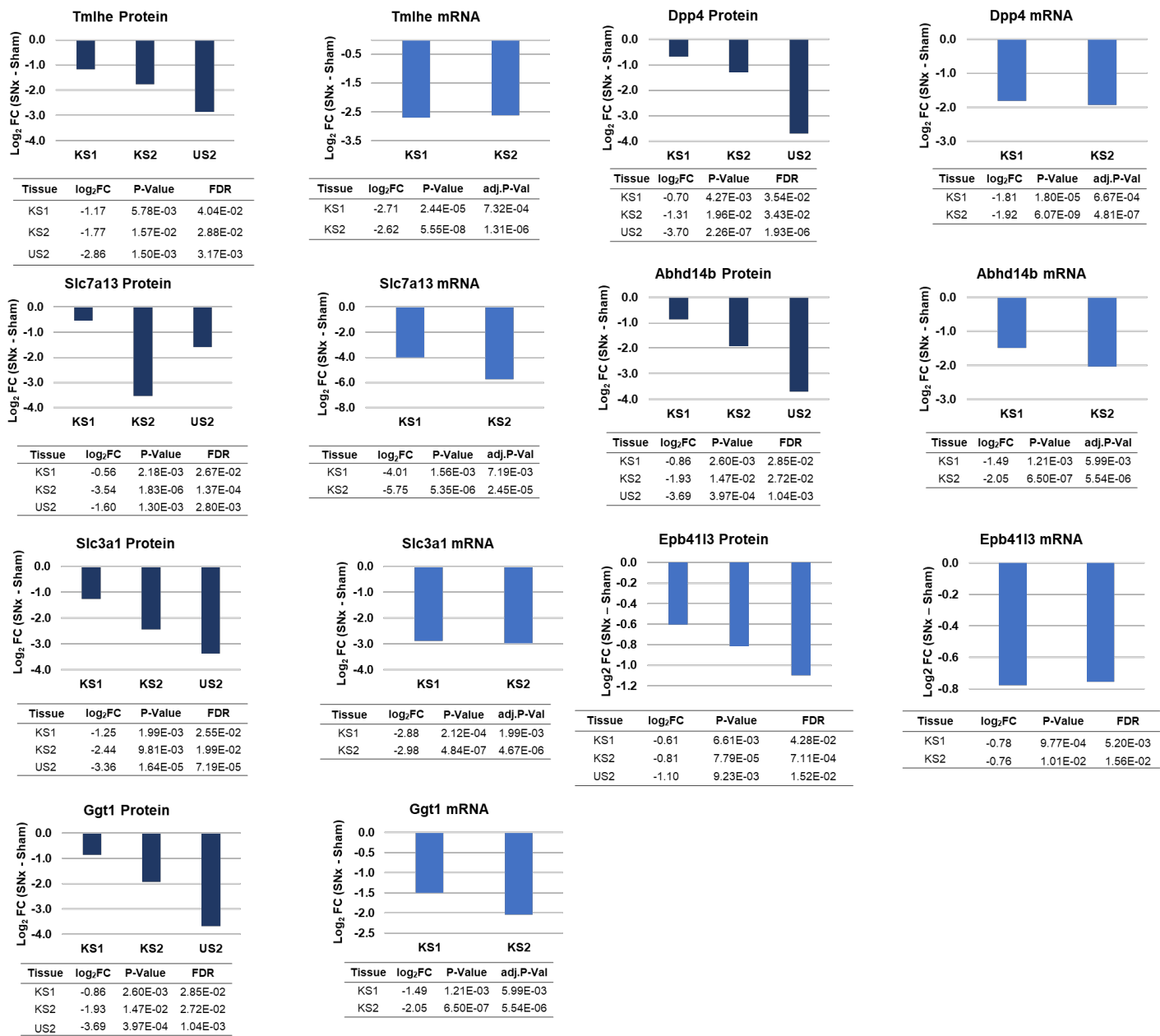


Supplementary Figure 7: Protein and gene expression of proteins in common in all proteomic and transcriptomic datasets. a) Additional up-regulated proteins (plasma proteins excluded). b) Down-regulated proteins.

a



b



Sic3a1 Protein

Tissue	log ₂ FC	P-Value	FDR
KS1	-1.25	1.99E-03	2.55E-02
KS2	-2.44	9.81E-03	1.99E-02
US2	-3.36	1.64E-05	7.19E-05

Sic3a1 mRNA

Tissue	log ₂ FC	P-Value	adj.P-Val
KS1	-2.88	2.12E-04	1.99E-03
KS2	-2.98	4.84E-07	4.67E-06

Epb4113 Protein

Tissue	log ₂ FC	P-Value	FDR
KS1	-0.61	6.61E-03	4.28E-02
KS2	-0.81	7.79E-05	7.11E-04
US2	-1.10	9.23E-03	1.52E-02

Epb4113 mRNA

Tissue	log ₂ FC	P-Value	FDR
KS1	-0.78	9.77E-04	5.20E-03
KS2	-0.76	1.01E-02	1.56E-02

Ggt1 Protein

Tissue	log ₂ FC	P-Value	FDR
KS1	-0.86	2.60E-03	2.85E-02
KS2	-1.93	1.47E-02	2.72E-02
US2	-3.69	3.97E-04	1.04E-03

Ggt1 mRNA

Tissue	log ₂ FC	P-Value	adj.P-Val
KS1	-1.49	1.21E-03	5.99E-03
KS2	-2.05	6.50E-07	5.54E-06

Supplementary Figure 8: Next Bio Human Kidney Disease gene expression database repository. Lumican and Col3a1 gene expression in kidneys compared to controls in diseased patients.

Next Bio database Human Kidney Disease

